Halsted, C.T., Bierman, P.R., Shakun, J.D., Davis, P.T., Corbett, L.B., Caffee, M.W., Hodgdon, T., and Licciardi, J., 2022, Rapid southeastern Laurentide Ice Sheet thinning during the last deglaciation revealed by elevation profiles of in-situ cosmogenic ^{10}Be: GSA Bulletin, https://doi.org/10.1130/B36463.1.

Supplemental Material

Table S1. New sample information: site parameters, sample preparation and analyses, age calculations

Table S2. Previously-published sample information: locations, publications, CRONUS entry information

Table S3. Blanks analysis, including ^{10}Be concentration calculations using batch-specific blank corrections vs. a project-averaged blank correction

Table S4. CRONUS Calculations: CRONUS setup, ages from different scaling schemes and production rate calibration datasets

Blanks

For the samples processed at University of Vermont (UVM), we performed a sensitivity test to assess two different ^{10}Be/^{9}Be blank corrections: a batch-by-batch correction and an overall average correction. This test demonstrated that our choice of batch-by-batch vs. project-averaged blank value had minimal impact on calculated ^{10}Be concentrations, with the differences between concentrations (<1%) well within the analytical uncertainty of measurements (typically 2 to 5%). We show this sensitivity test in Table S3.

We had one blank with a higher than usual ^{10}Be/^{9}Be ratio: UVM batch 621 blank with ^{10}Be/^{9}Be ratio of $2.26*10^{-14}$. All other blanks have ^{10}Be/^{9}Be ratios equal to or less than $1*10^{-15}$. The batch 621 blank is a clear outlier, its ^{10}Be/^{9}Be ratio is more than 60 standard deviations away from the mean of the other 13 blanks. Given the consistency of blanks from UVM batches before and after batch 621, we suspect that material from a batch 621 sample was introduced to the blank at some point during processing; therefore, we omitted it from the overall average. Because of this, we use the average ^{10}Be/^{9}Be ratio from the other 13 blanks as the batch-specific blank value for batch 621 during our sensitivity analysis.

We also had two blanks with zero ^{10}Be counts (UVM batches 685 and 694), making it impossible to exactly quantify ^{10}Be in the blanks. To estimate the ^{10}Be/^{9}Be ratio of the zero-count blanks, we combined the measurements (run time, ^{9}Be current, ^{10}Be counts) from other blanks using the same Be carrier and run on the AMS at the same time and calculate a 'combined blank' value.

For the purposes of the concentrations and ages presented in the manuscript, we use the project-averaged blank ^{10}Be/^{9}Be ratio value of $5.8*10^{-16} \pm 3.2*10^{-16}$ (value does not include the blank from batch 621) to correct the sample ratios. Using this value for all samples avoids any potential complications from treating samples from some batches (621, 685, 694) differently than others due to their batch blanks having statistically implausible values. Additionally, our

sensitivity test demonstrates that the choice between batch-by-batch and project-averaged blank values has minimal impact on calculated ^{10}Be concentrations and ages. This average blank likely does a more effective job than a batch-by-batch blank at capturing the blank uncertainty due to the large number of measurements included.

Thinning Rate Calculations

We use regressions between sample exposure ages and elevations in a Monte Carlo random resampling framework to evaluate a range of possible ice thinning rates at each mountain. In each regression, exposure ages assume a randomly assigned value from within their range of analytical uncertainty (assuming a Gaussian uncertainty distribution) and a least-squares best fit line is fitted to the elevation/randomized-age data. We program a filter into the Monte Carlo regressions so that best-fit lines indicating ice thickening over time are discarded. We discard samples from regressions if their exposure age does not overlap within external uncertainty (analytical + production rate uncertainties) with nearby, independent deglacial constraints such as radiocarbon or calibrated varve chronologies (see results section in main text). In these cases, we assume that exposure ages do not reflect local deglaciation due to inherited nuclides increasing apparent ages, post-glacial shielding decreasing apparent ages, or post-glacial movement of boulder samples causing ages to post-date glaciation.

Our calculated thinning rates cover a wide range of plausible values. The 95% confidence intervals for most vertical transects range from 0.1 to >4 m/yr and some transects have plausible rates of more than 10 m/yr (Figs S1, S2). We attribute this inability to tightly constrain plausible thinning rates to indistinguishable ages over most of the transects. Such wide ranges for thinning rates are calculated for other vertical exposure age transects that have indistinguishable ages from top to bottom (e.g., Johnson et al., 2014; Small et al., 2019).

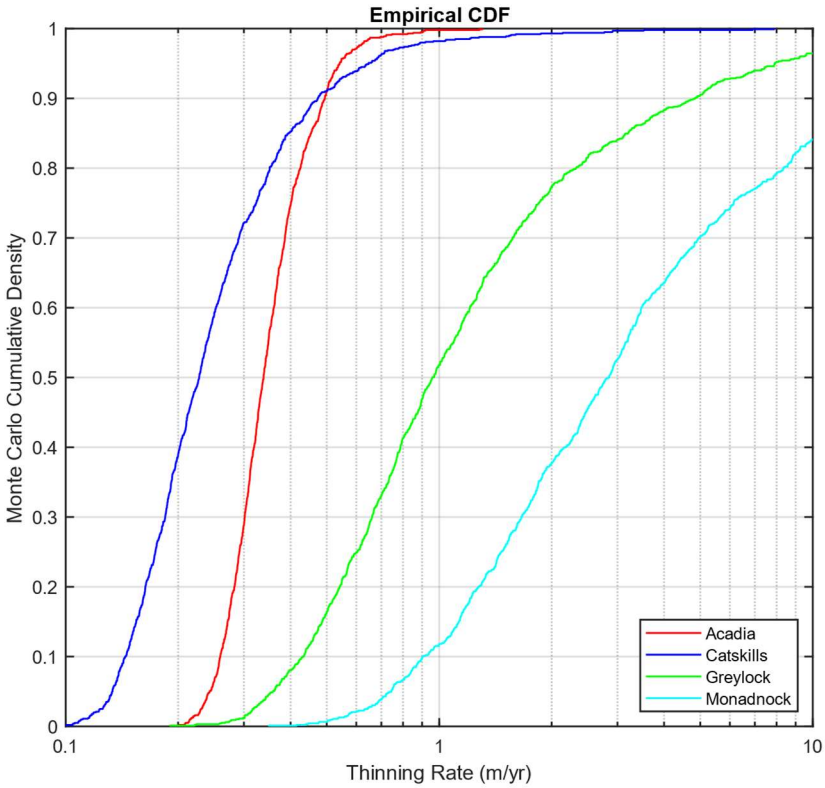

Figure S1: Cumulative density function plot of thinning rates from exposure age/elevation Monte-Carlo regressions of vertical transects from LIS peripheral sites

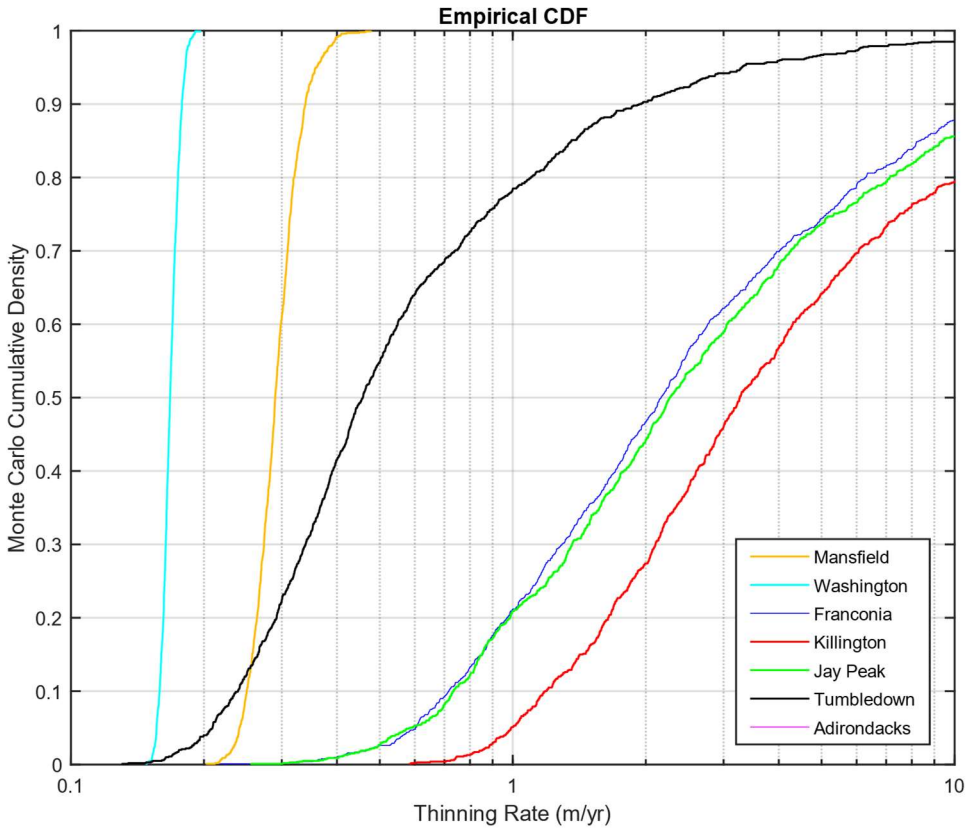

Figure S2: Cumulative density function plot of thinning rates from exposure age/elevation Monte-Carlo regressions of vertical transects from LIS up-ice sites

Transect Maps

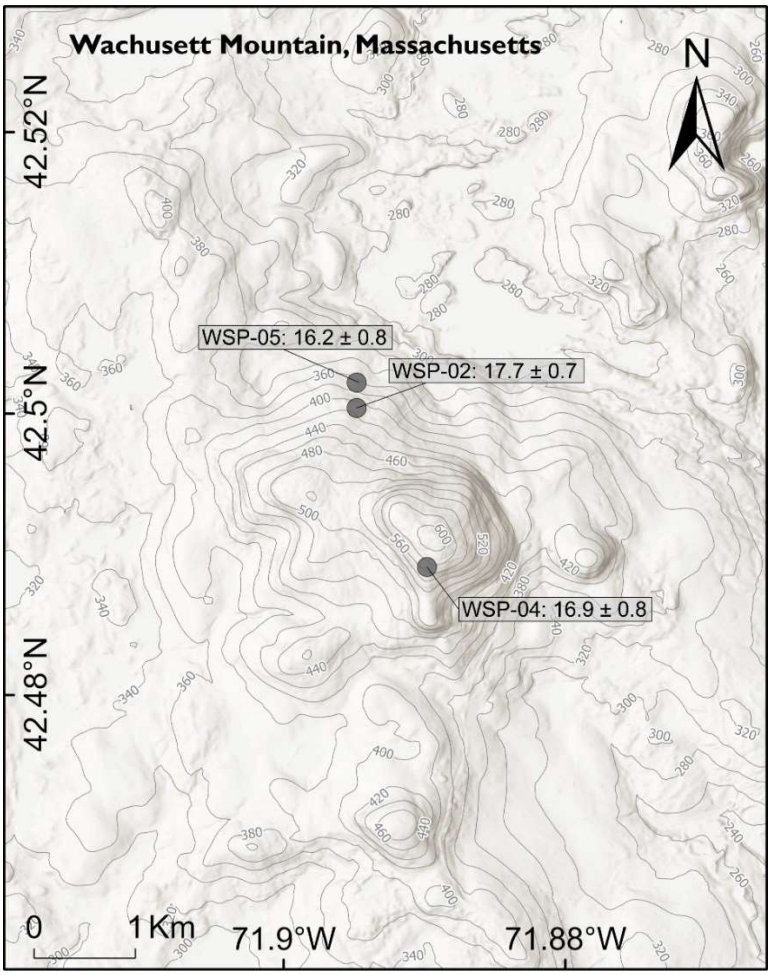
Wachusett Mountain, Massachusetts
N
WSP-05: 16.2 ± 0.8
WSP-02: 17.7 ± 0.7
WSP-04: 16.9 ± 0.8
42.52°N
42.5°N
42.48°N
71.9°W
71.88°W
0
1Km

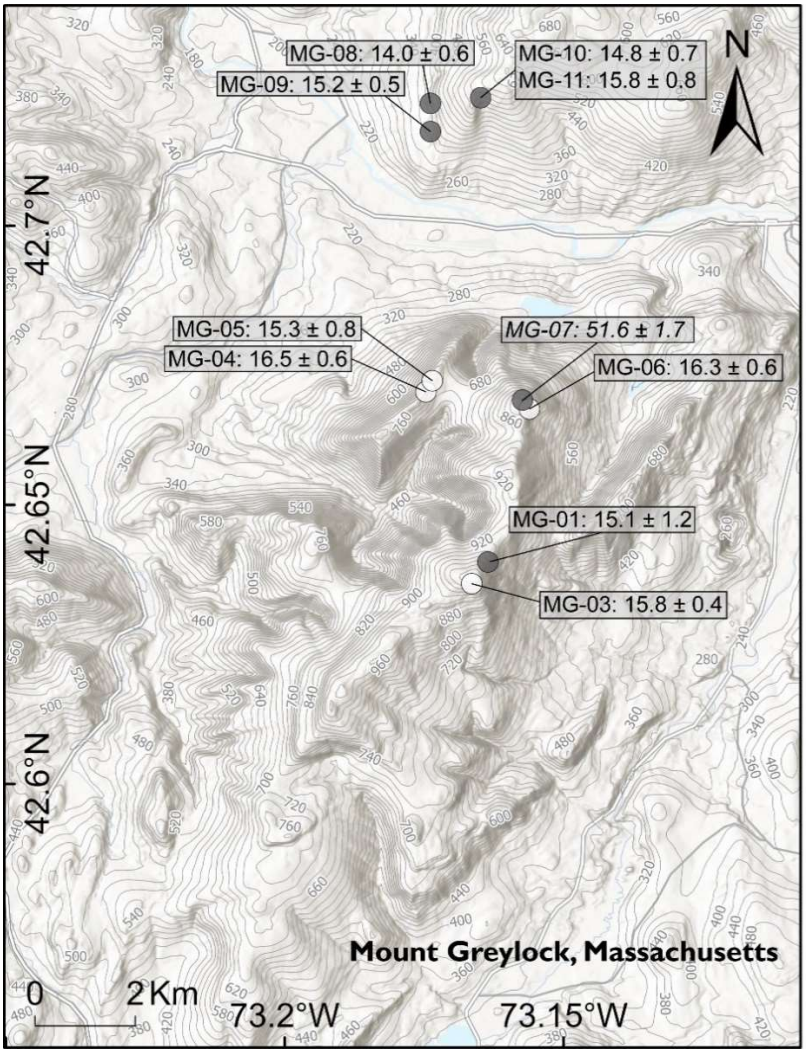
MG-08: 14.0 ± 0.6
MG-10: 14.8 ± 0.7
MG-09: 15.2 ± 0.5
MG-11: 15.8 ± 0.8
N
MG-05: 15.3 ± 0.8
MG-07: 51.6 ± 1.7
MG-04: 16.5 ± 0.6
MG-06: 16.3 ± 0.6
MG-01: 15.1 ± 1.2
MG-03: 15.8 ± 0.4
42.7°N
42.65°N
42.6°N
Mount Greylock, Massachusetts
0
2Km
73.2°W
73.15°W

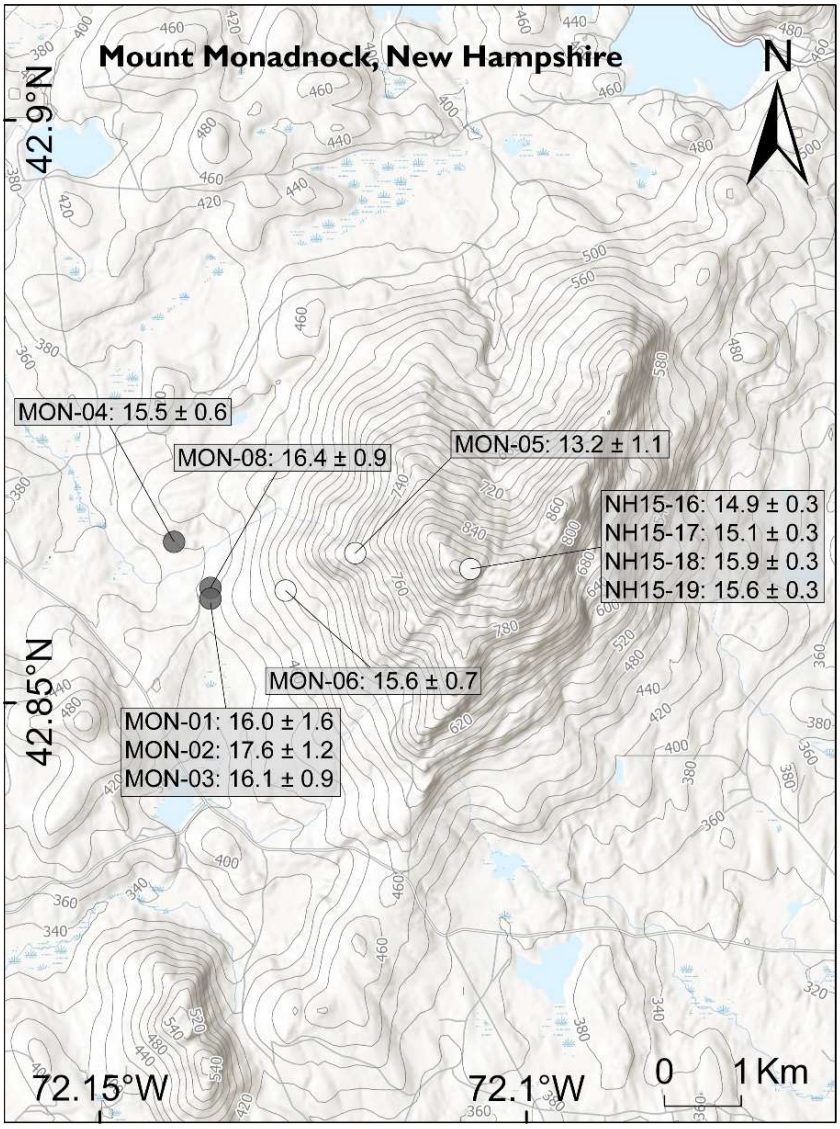
Mount Monadnock, New Hampshire
N
42.9°N
42.85°N
72.15°W
72.1°W
0
1 Km
MON-04: 15.5 ± 0.6
MON-08: 16.4 ± 0.9
MON-05: 13.2 ± 1.1
NH15-16: 14.9 ± 0.3
NH15-17: 15.1 ± 0.3
NH15-18: 15.9 ± 0.3
NH15-19: 15.6 ± 0.3
MON-06: 15.6 ± 0.7
MON-01: 16.0 ± 1.6
MON-02: 17.6 ± 1.2
MON-03: 16.1 ± 0.9

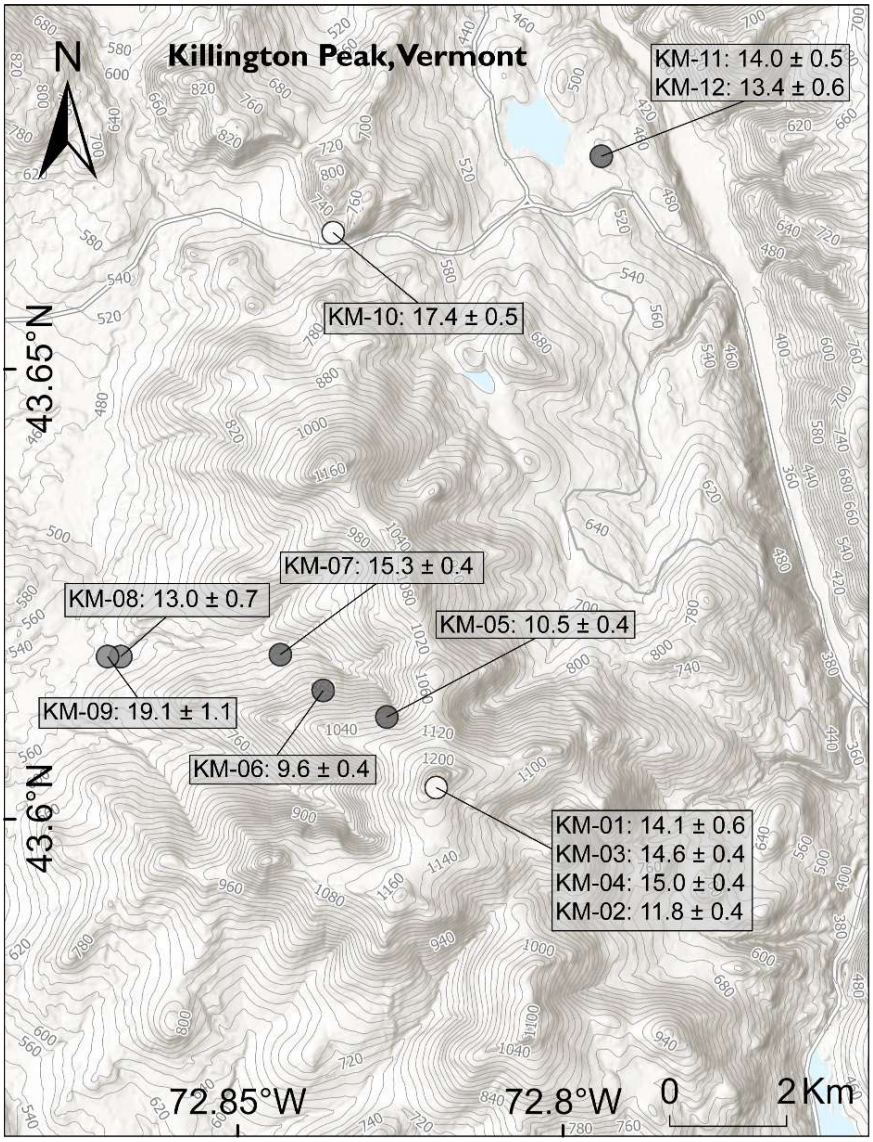
Killington Peak, Vermont
N
KM-11: 14.0 ± 0.5
KM-12: 13.4 ± 0.6
KM-10: 17.4 ± 0.5
KM-07: 15.3 ± 0.4
KM-08: 13.0 ± 0.7
KM-05: 10.5 ± 0.4
KM-09: 19.1 ± 1.1
KM-06: 9.6 ± 0.4
KM-01: 14.1 ± 0.6
KM-03: 14.6 ± 0.4
KM-04: 15.0 ± 0.4
KM-02: 11.8 ± 0.4
43.65°N
43.6°N
72.85°W
72.8°W
0
2 Km

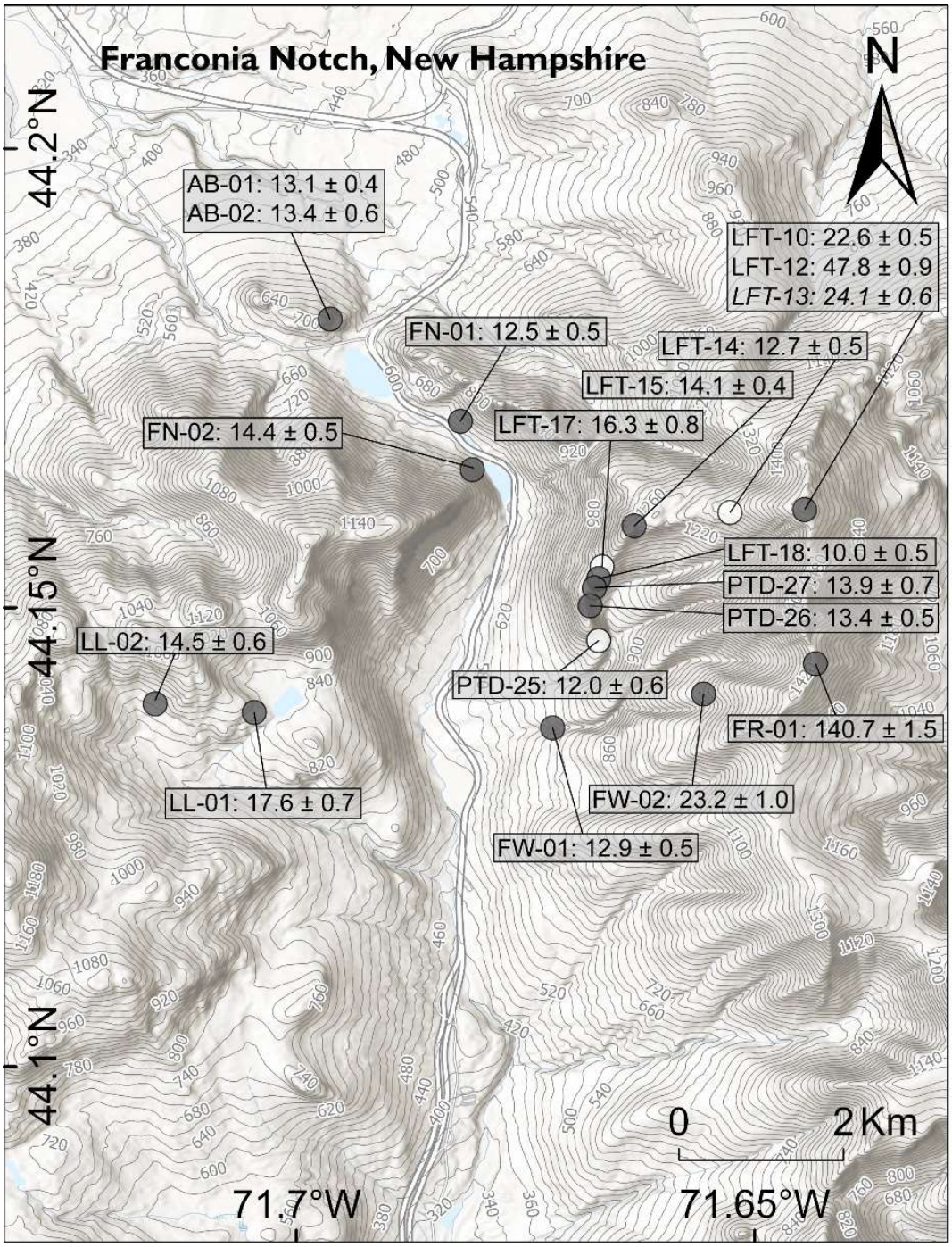
Franconia Notch, New Hampshire
N
AB-01: 13.1 ± 0.4
AB-02: 13.4 ± 0.6
LFT-10: 22.6 ± 0.5
LFT-12: 47.8 ± 0.9
LFT-13: 24.1 ± 0.6
FN-01: 12.5 ± 0.5
LFT-14: 12.7 ± 0.5
LFT-15: 14.1 ± 0.4
LFT-17: 16.3 ± 0.8
FN-02: 14.4 ± 0.5
LFT-18: 10.0 ± 0.5
PTD-27: 13.9 ± 0.7
PTD-26: 13.4 ± 0.5
LL-02: 14.5 ± 0.6
PTD-25: 12.0 ± 0.6
FR-01: 140.7 ± 1.5
LL-01: 17.6 ± 0.7
FW-02: 23.2 ± 1.0
FW-01: 12.9 ± 0.5
44.2°N
44.15°N
44.1°N
71.7°W
71.65°W
0
2 Km

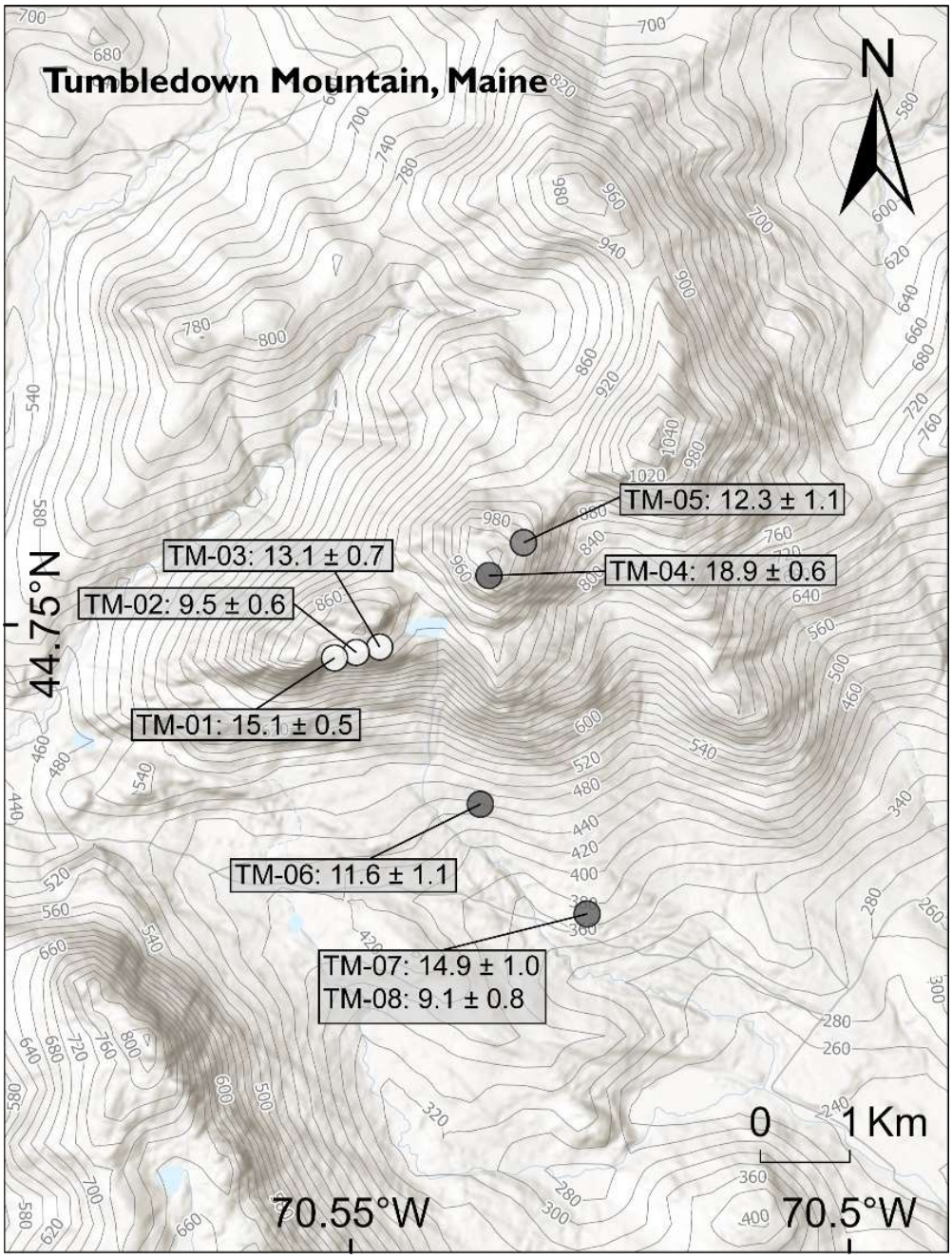
Tumbledown Mountain, Maine
N
TM-05: 12.3 ± 1.1
TM-04: 18.9 ± 0.6
TM-03: 13.1 ± 0.7
TM-02: 9.5 ± 0.6
TM-01: 15.1 ± 0.5
TM-06: 11.6 ± 1.1
TM-07: 14.9 ± 1.0
TM-08: 9.1 ± 0.8
44.75°N
0
1 Km
70.55°W
70.5°W

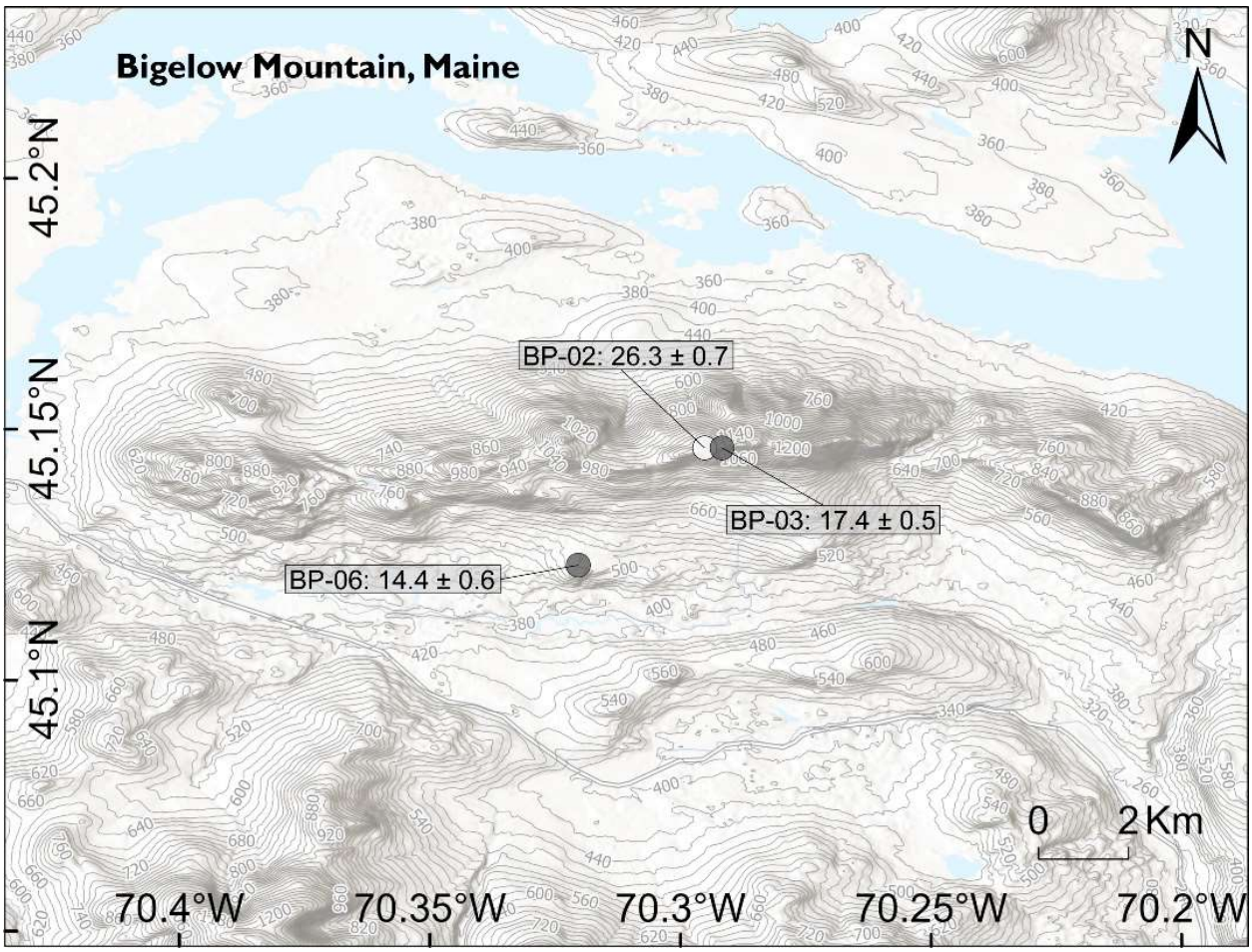
Bigelow Mountain, Maine
N
BP-02: 26.3 ± 0.7
BP-03: 17.4 ± 0.5
BP-06: 14.4 ± 0.6
0
2 Km
45.2°N
45.15°N
45.1°N
70.4°W
70.35°W
70.3°W
70.25°W
70.2°W

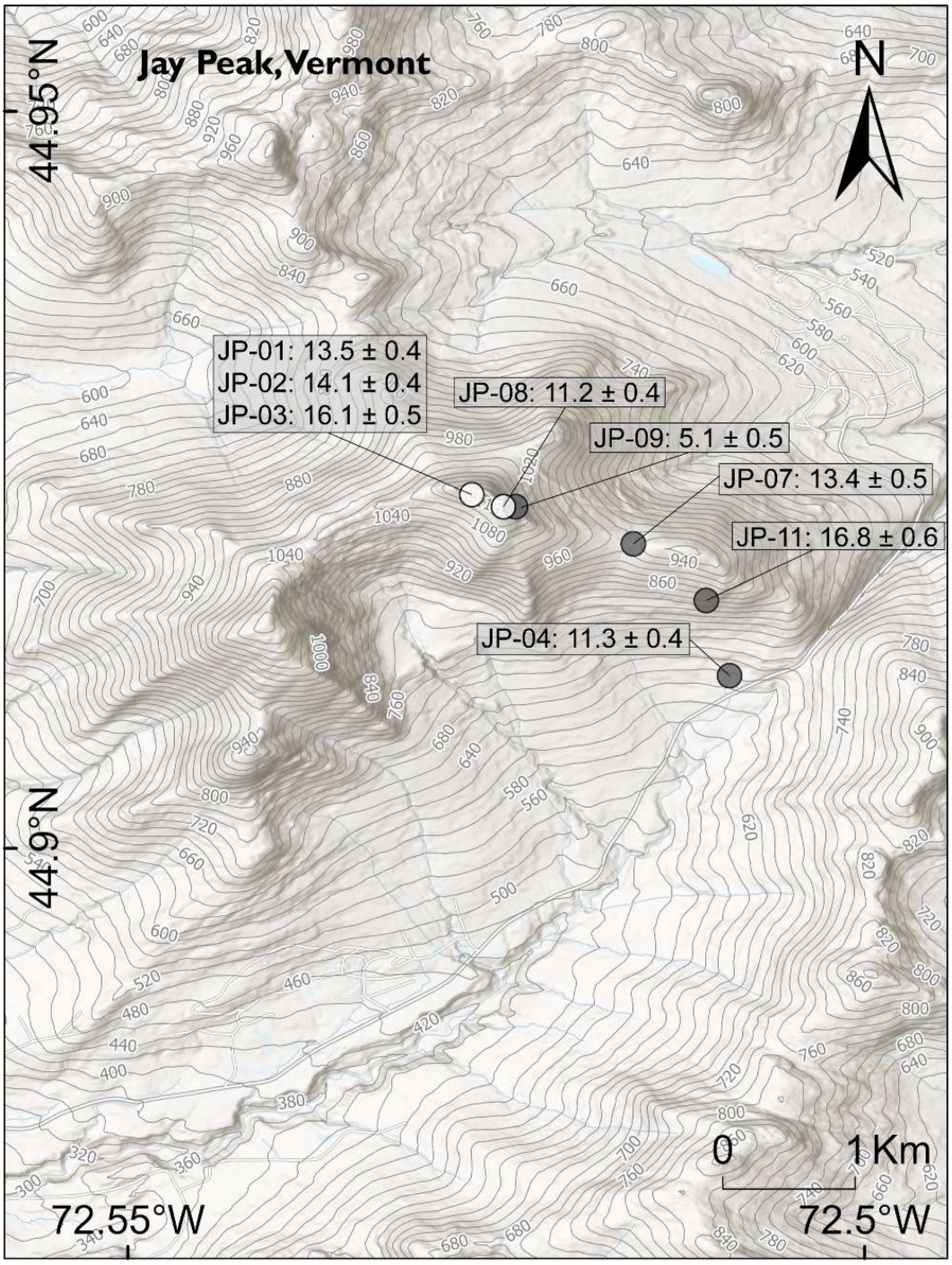
Jay Peak, Vermont
N
44.95°N
44.9°N
72.55°W
72.5°W
0
1Km
JP-01: 13.5 ± 0.4
JP-02: 14.1 ± 0.4
JP-03: 16.1 ± 0.5
JP-08: 11.2 ± 0.4
JP-09: 5.1 ± 0.5
JP-07: 13.4 ± 0.5
JP-11: 16.8 ± 0.6
JP-04: 11.3 ± 0.4